Failure modes in FRCM systems with dry and pre-impregnated carbon yarns: experiments and modeling

Jacopo Donnini[1], Giovanni Lancioni[2], Valeria Corinaldesi[3]

[1] Dipartimento di Scienze e Ingegneria della Materia, dell'Ambiente ed Urbanistica, Università Politecnica delle Marche, Ancona, Italy, j.donnini@univpm.it
[2] Dipartimento di Ingegneria Civile, Edile e Architettura, Università Politecnica delle Marche, Ancona, Italy, g.lancioni@univpm.it
[3] Dipartimento di Scienze e Ingegneria della Materia, dell'Ambiente ed Urbanistica, Università Politecnica delle Marche, Ancona, Italy, v.corinaldesi@univpm.it

ABSTRACT

Fiber Reinforced Cementitious Matrix (FRCM) systems have emerged in recent years as an effective tool for strengthening and retrofitting of the existing built heritage.
The effectiveness of FRCM systems is strongly related to the bond developed at the interface between inorganic matrix and fabric reinforcement and between the inorganic matrix and the substrate. However, since the major weakness is often located at the matrix-to-fiber interface, the study of stress-transfer mechanisms between fibers and matrix, and a better understanding of the failure processes become of fundamental importance.
In this paper, interface bond-slip relations are derived from pull out tests on multifilament carbon yarns embedded in a cementitious matrix. Two different types of yarns are investigated, dry and pre-impregnated with epoxy resin. A variational model able to reproduce the mechanisms of interface debonding and frictional slippage observed in experiments is developed, where the constitutive parameters are calibrated on the base of the experimental data available from pull out tests. The model is implemented in a finite elements code, and pull out and double shear bond tests on masonry substrates are simulated. Finally, numerical results are compared with experimental evidences.

Keywords:

FRCM, carbon yarn, bond-slip law, debonding, slippage, variational modeling.

1. Introduction

In the last few years, the growing need to recover, reinforce and strengthen existing masonry or concrete buildings led to the development of innovative materials and new repair techniques with low environmental impact and high efficacy. Fiber Reinforced Cementitious Matrix (FRCM), also called Textile Reinforced Mortar (TRM), applied as external reinforcement and acting as an additional tensile-resistant element, proved to be very effective in increasing both mechanical strength and ductility of masonry and concrete structures.

FRCM are generally constituted by uni-directional or bi-directional fabrics, consisting of multifilament yarns made of carbon, glass, basalt or PBO fibers, disposed along two orthogonal directions. If compared to organic matrix systems (e.g. FRP, SRP) the use of a cementitious or lime-based matrix guarantees better compatibility with concrete or masonry substrates, higher breathability and vapor permeability, high temperature resistance, applicability on wet and irregular surfaces, more security for operators during installation [1-4].

FRP and FRCM are similar in the way they are designed as external reinforcement for structures or elements that need to be strengthened. However, while the performances of FRP are strongly influenced by the effectiveness of the stress transfer mechanisms from the substrate to the composite, since the failure often occurs before the ultimate tensile strength of the composite is reached [5-6], FRCM performances are more affected by the stress transfer mechanisms at the interface between fabric reinforcement and inorganic matrix, since the failure is often expected at this interface.

The FRCM mechanical behavior and failure mode are strongly dependent on the type of fabric reinforcement used. Fabrics are usually constituted by yarns made of dry filaments but often they are coated or pre-impregnated with organic compounds in order to improve the adherence with the inorganic matrix. In this context, the term coating is intended for a superficial impregnation of the yarn fibers, with the inner filaments of the bundle left dry, while pre-impregnation indicates a complete impregnation of the yarn with organic resins.

In case of fabric reinforcement made of multifilament dry yarns, FRCM properties are influenced by the ability of the inorganic matrix to penetrate within the filaments. Since the matrix is able to engage only the external fibers of the yarns, the so called ‘telescopic’ behavior, due to slippage of the internal filaments of the yarn, is activated [7].

In case of coated or pre-impregnated yarns, the penetration of the mortar within the filaments is prevented by the presence of the organic resin. As a consequence, the bond between yarn and matrix is no longer dependent on the ability of the mortar to penetrate within the filaments but rather from the bond at the interface between coating and matrix [8,9]. In this case it is possible to precisely identify a contact surface between yarn and matrix, while in case of dry yarns it is not easy to establish how many filaments are engaged in the stress transfer mechanisms. In fact, the ability of the mortar to penetrate between the filaments depends on many factors, such as mortar viscosity, size of the aggregates or fillers that constitute the mortar, space between filaments and also by the technique used to apply the FRCM to the substrate (trowel, plastering machine). Thus two different types of bond are distinguished in multifilament dry yarns: bond between filaments and matrix and bond between filaments. In case of pre-impregnated yarns the slippage between filaments is prevented by the resin and only the bond between yarn and cementitious matrix is considered.

In this scenario, the definition of an appropriate bond-slip law (BSL) for a given FRCM system is fundamental to allow the development of analytical or numerical models able to simulate the FRCM mechanical behavior and failure modes.

The bond between multifilament yarns and cementitious matrix has been studied by several authors by using different methodologies. Banholzer and coworkers proposed two different methods: the so called ‘direct method’, which requires the knowledge of an idealized BSL or the measurement of the longitudinal strain along the interface between yarn and matrix [10] and the ‘indirect method’, that is able to predict a BSL based on experimental parameters obtained by means of pull out, single or double shear bond tests on FRCM systems [11].

An indirect method to calibrate the cohesive material law of FRCM-concrete joints was proposed by Focacci and coworkers [12]. The method is based on single-lap shear bond tests on FRCM-concrete joints with different bonded lengths, using the peak load versus bonded length to calibrate the BSL. Other models based on the analysis of the shear stress at the interface yarn-matrix in pull out [13,14] or single shear tests [15-19] have been proposed in the literature. However, all these studies have shown that measuring the fiber strain in FRCM composites is a difficult task, due to the presence of the matrix embedding the fabric yarns, while using idealized BSL is not always able to accurately describe the FRCM mechanical behavior.

In this work a different approach has been proposed, by using simple pull out tests on single yarns to calibrate the BSL, for different FRCM systems.

During pull out test on a single yarn embedded in a cement matrix, force and slip at the loaded end can be easily measured. As a result, the relationship between the shear stress and the slip along the interface (BSL) can be derived by considering the shear stress to be constant along the interface with no need to apply strain sensors on the yarn surface. This assumption is acceptable for short embedded lengths (equal to 20 mm), as confirmed by experimental and numerical results, while it is no longer reliable for higher lengths.

Two types of carbon yarns, dry and fully pre-impregnated with an organic resin, have been used, these two representing the antipodes of what is currently on the market of FRCM systems. As a consequence, two different BSL have been obtained from pull out tests.

A variational model has been developed and implemented in a finite element code to simulate the possible failure mechanisms of FRCM systems reinforced with these two types of carbon fabrics.

Following a phase-field approach [20], the proposed model is based on an energy functional which depends on a damage parameter α ranging from 0 to 1 (α=0 means sound material, and α=1 means totally damaged material), which accounts for possible fracture of the constituents (cementitious matrix and carbon reinforcement), or debonding and slippage at the yarn-to-matrix interface. Different energies have been assigned to the system constituents and to the interface. Regarding matrix and yarn, the energy proposed in [21,22] has been considered. It incorporates a linear local damage term and a non-local damage contribution in order to describe the behavior of brittle materials. The energy assigned to the yarn-to-matrix interface is constituted by three terms: (1) an elastic contribution, which accounts for a distribution of elastic springs whose elastic stiffness degrades when damage increases, (2) a local damage term, accounting for debonding, and (3) a frictional energy, expended in the phase of slippage that follows the detachment. This third term is similar to that proposed in [23,24] to model plastic slip flow, and it only depends on one parameter, τ_0, which represents the frictional shear stress. The corresponding parameter in [23] represented the plastic yielding stress.

It follows that the three energy terms are directly related to the three basic phases of the failure process at the yarn-to-matrix interface observed in experiments, i.e., the initial elastic shear, the debonding in a regime of stress-softening, and the slippage occurring at constant frictional shear stress. This strict correlation is a distinguishing feature of the proposed formulation, with respect to the model proposed in [25], where a unique damage energy was considered to describe the post-elastic evolution.

Two different failure modes, brittle and ductile with a softening phase, have been observed for dry and pre-impregnated carbon yarns, respectively. To account for these differences, two expressions of the damage energy have been considered: a concave function of α, to capture brittle damaging, and a linear function to describe the softening phase.

Evolution of strain and damage, as the external load increases, is determined by solving a constrained incremental minimization problem, that has been implemented in a sequential

quadratic programming algorithm. Incremental minimization was used to determine local minima in many different evolution problems concerning fracture [26], plasticity [27,28] or crystal plasticity [29].
Experimental data have been used to calibrate the constitutive parameters that characterize the interface, such as the shear elastic stiffness k, the peak shear stress τ_e and the frictional shear stress τ_0. They have been easily derived from the experimental force-displacement curves of pull out tests. Once the model has been calibrated, numerical simulations have been carried out. Both pull out and double shear bond tests have been reproduced by considering different bond lengths. Interface debonding and slippage have been investigated in the two cases of dry and pre-impregnated yarns, and comparisons with experimental results have been carried out.

The paper is organized as follows:
Experimental results of pull out tests on specimens made of dry or pre-impregnated carbon yarns embedded in a cementitious matrix are presented in Section 2. The effect of varying the bond length is also discussed.
In Section 3 a phase-field model has been developed in order to reproduce the FRCM mechanical behavior, taking into account the possible failure of the constituent materials, the slippage at the yarn to the matrix interface and the frictional stress in the post-elastic phase. The bond parameters have been calibrated, based on experimental results, and implemented within the model.
Pull out tests and double shear bond test have been simulated in Section 4. The effect of varying the bond length of the carbon yarn or fabric within the inorganic matrix and the use of dry or pre-impregnated carbon yarns was also considered. Finally, numerical results have been compared with experimental outcomes in terms of load-displacements curves.

2. Experiments

2.1 Pull out test

A commercially available cementitious mortar with a maximum aggregates size of 0.5 mm has been used as FRCM matrix. Mechanical properties were investigated by means of three-point bending tests on standard prisms (40x40x160 mm) and compressive tests on the two remaining broken parts. Tests were performed after 28 days of casting at 20 °C and 50% RH. Two different types of carbon yarn were used: the first one constituted by multifilament dry carbon fibers (DRY) and the second realized by applying a complete organic pre-impregnation (IMP). The pre-impregnation consisted on a fully saturation of the yarn with flexible epoxy resin and a thin layer of quartz sand (maximum sand size of 1 mm) applied to the surface. Tensile strength and elastic modulus of the carbon yarn were evaluated by means of tensile tests, according to ISO 10618. Material properties of cementitious mortar and carbon yarn are collected in Table 1.
A total of 25 pull out tests were carried out on specimens made of dry or coated carbon yarns embedded in a cylinder of cementitious mortar (diameter D=50 mm) with different embedded lengths (h=20÷50 mm). The pull out test setup is illustrated in Figure 1. Specimens have been labelled by indicating the type of carbon yarn, DRY or pre-impregnated (IMP), followed by the embedded length (h). The free length l is kept constant and equal to 80 mm. Pull out tests were performed using a tensile testing machine with a load bearing capacity of 50 kN. The specimen is fixed at the top by a metallic frame anchored to the testing machine and the yarn is gripped and pulled in displacement control at 0.5 mm/min. The displacement s_e, corresponding to the maximum force f_{max}, was calculated by subtracting the elastic deformation of the bare yarn to the

total displacement d_e, measured at the head of the testing machine: $s_e = d_e - f_{max} l / (A_f E_f)$, where E_f is the Young's modulus of the carbon yarn, and A_f is the yarn cross-section area.

Table 1 - Material properties

Material	Compressive strength (MPa)	Tensile strength σ_e (MPa)	Elastic modulus E (GPa)	Unit weight (kg/m^3)	Poisson ratio ν
Cementitious mortar (*m*)	45	6.2	34.5	1320	0.2
Carbon fiber	-	4900	240	-	0.3
Carbon yarn (*f*)	-	1850	150	-	0.3

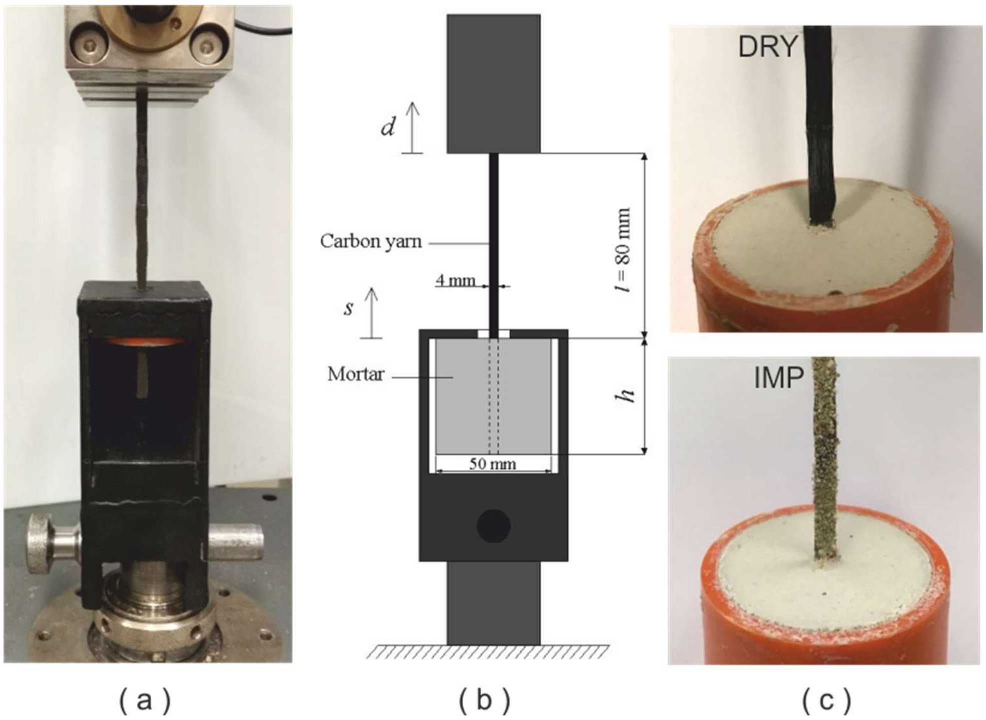

Figure 1 - Pull out test set up (a), geometrical scheme (b), dry and pre-impregnated carbon yarns (c).

Experimental results of pull out tests are reported in Table 2. The average maximum load f_{max} was evaluated on 5 specimens for each type of geometry while s_e represents the corresponding displacement. Three experimental pull out curves for each type of specimen are reported in Figure 2, while the grey region represents the envelope of all experimental curves which have been used to derive the bond parameters: τ_e, τ_0, k.

The maximum shear stress τ_e at the interface is supposed to be constant along the embedded length. This value is estimated through the formula $\tau_e = f_{max} / (h \cdot p)$, where p is the perimeter of the yarn equal to 8.64 mm and h is the embedded length.

The frictional shear stress τ_0 has been evaluated as the stress corresponding to the pure frictional phase of the pull out curve. τ_0 represents the shear stress at s=3 mm, since at this point it is sure that the yarn is completely debonded from the matrix and the pull out is governed only by frictional stresses at the interface. In case of dry yarns τ_0 is assumed equal to zero.

The shear modulus is $k=\tau_e/s_e$.

Table 2 - Experimental results of pull out tests

Specimen		f_{max} (N)	s_e (mm)	τ_e (MPa)	τ_0 (MPa)	k (N/mm^3)
DRY_20	Average	242	0.44	1.40	0	3.10
	CoV (%)	*14.2*	*11.5*	*14.2*	-	*14.3*
DRY_50	Average	479	0.72	1.11	0	1.54
	CoV (%)	*6.0*	*15.1*	*6.0*	-	*13.2*
IMP_20	Average	342	0.5	1.98	1.25	3.95
	CoV (%)	*7.9*	*13.7*	*7.9*	*7.3*	*9.2*
IMP_30	Average	501	0.77	1.93	1.28	2.51
	CoV (%)	*6.8*	*17.3*	*6.8*	*4.7*	*14.7*
IMP_50	Average	748	0.95	1.73	1.25	1.82
	CoV (%)	*8.9*	*14.3*	*8.9*	*3.2*	*11.8*

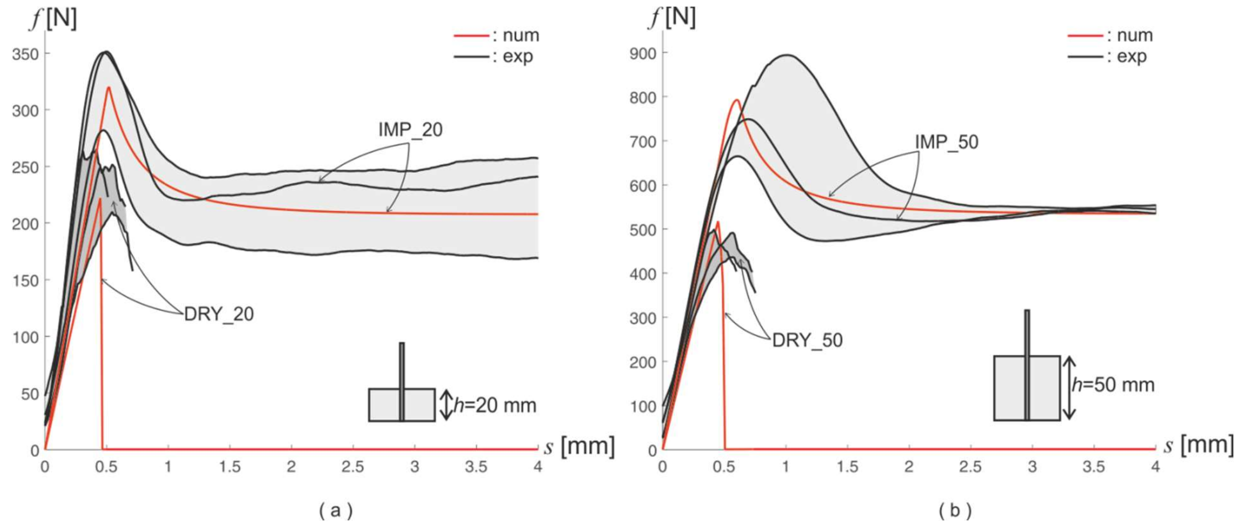

Figure 2 - Experimental and numerical load-displacement curves of pull out tests.

Load-displacement curves reported in Figure 2 show a substantial increase of the maximum load f_{max} passing from dry to pre-impregnated (IMP) carbon yarn. The pre-impregnation has a major influence on the quality of the adhesion between yarn and matrix and allows for a more uniform distribution of the stresses all over the yarn cross section. The pull out resistance increases about 40% and 55% for an embedded length of 20 and 50 mm, respectively.

It can be observed that the maximum load f_{max} increases by increasing the embedded length h while the shear stress τ_e calculated over the total length of the interface decreases. The reduction of the stress value τ_e by increasing the embedded length explains in part why the distribution of the shear stress along the interface cannot be considered constant for longer (>20 mm) embedded lengths. The debonding at the interface yarn-to-matrix propagates slowly from the top of the specimen. In case of short embedded length this propagation is fast, and stress distribution along the interface, once the maximum load is reached, can be considered almost constant. This phenomenon has been confirmed by numerical simulations.

In the case of dry yarns no frictional shear stress in the post-elastic phase was observed: the behavior is elastic-brittle with a sudden drop of the load after exceeding the maximum load.

For pre-impregnated carbon yarns (IMP), when the maximum shear stress τ_e is reached, the softening phase takes place and the shear stress decreases. During this phase the yarn begins to detach from the matrix at the top of the specimen, up to reach the complete debonding through the interface. After that, the shear stress becomes constant, while the slippage of the yarn within the matrix is governed only by the frictional stress τ_0. The value of τ_0 is about 35% lower than the maximum shear stress τ_e.

It can be observed that τ_0 does not vary by changing the embedded length and so it can be considered as a material parameter which depends only on the bond quality of the interface between yarn and matrix.

2.2 SEM analysis

The interface between dry (Figures 3a,b) or pre-impregnated (Figures 3c,d) carbon yarn and the surrounding mortar was observed by SEM (at magnifications ranging from 20× to 100×), on specimens after pull out test. It is clear to observe that the inorganic matrix doesn't penetrate within the dry carbon filaments and it is able to engage only the external carbon filaments. The inner filaments are pulled out of the matrix while only few external filaments remain attached to the matrix. In pre-impregnated carbon yarns, the penetration of the mortar within the filaments is prevented by the resin (Figure 3c). However, the mortar is able to completely wrap the yarn, ensuring a better interface quality. After the specimen has been tested in pull out it can be observed a clear debonding at the yarn to mortar interface. A non-perfect impregnation of the inner filaments of the yarn can also be observed in Figure 3d. In some cases, the sand grains used to improve the adhesion within yarn and matrix remain attached to the surrounding mortar more than to the yarn surface, due to their considerable size, if compared to the yarn cross section. This might suggest to apply a sand or powder of smaller size to increase the adhesion at the interface.

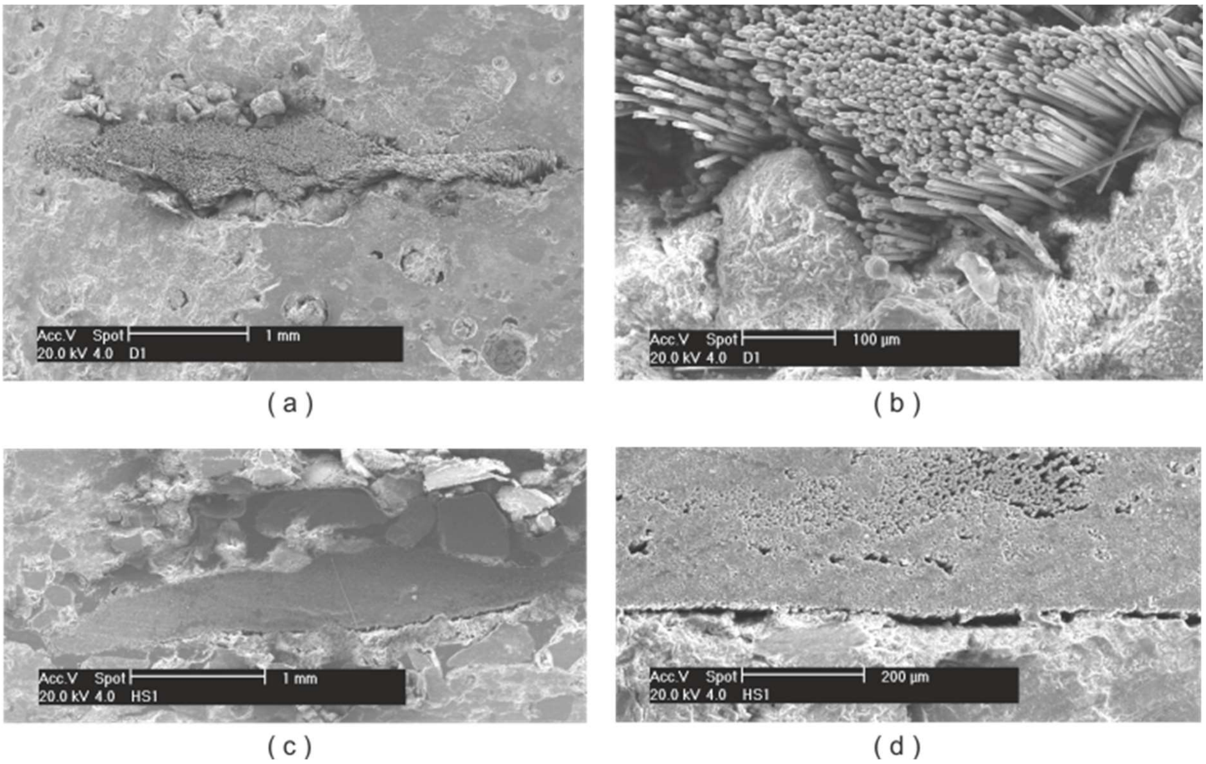

Figure 3 - SEM analysis at the yarn to matrix interface after pull out test, at different magnifications: Dry yarn (3ab); Pre-impregnated yarn (3cd).

3. Variational model

A composite body constituted by the subdomains Ω_m and Ω_f, representing the matrix and the yarn, has been considered, with Λ which represents the matrix-to-yarn interface (see Figure 6 for two-dimensional geometrical schemes of pull out and double shear bond tests). The multifilament yarn is considered as an homogeneous body, so that the shear between filaments and the so-called telescopic behavior are neglected. A monotonically increasing displacement s is applied on a portion $\partial_s\Omega_f$ of the yarn domain, and it constitutes the evolution parameter of the problem. The problem unknowns are the displacement $\mathbf{u}_s(x)$ and the damage $\alpha_s(x)$, which depend on the position x and on the imposed displacement s. Damage $\alpha_s(x)$ is a scalar field ranging from 0 to 1: α=0 means that the material is sound, and α=1 that it is totally damaged.

3.1 Energies

As in [22], the internal energy of the system is assumed to be sum of three contributions

$$\mathsf{E}(\mathbf{u}_s,\alpha_s)=\int_{\Omega_m}\varphi_m(\mathbf{u}_s,\alpha_s)dx+\int_{\Omega_f}\varphi_f(\mathbf{u}_s,\alpha_s)dx+\int_{\Lambda}\varphi_\Lambda(\boldsymbol{\delta}_s,\alpha_s)da, \qquad (1)$$

which correspond to the energies of matrix, yarn and interface. In the third integral, $\boldsymbol{\delta}_s$ is the displacement jump at the interface, that is, $\boldsymbol{\delta}_s(x)=\mathbf{u}_s^f(x)-\mathbf{u}_s^m(x)$, with $\mathbf{u}_s^m(x)$ and $\mathbf{u}_s^f(x)$ the displacement on the yarn and matrix boundaries, respectively. Since volume loads and surface loads at the boundary are assumed to be null, energy (1) represents the total energy of the system.

(i) Matrix and yarn energy densities

The matrix and yarn energy densities φ_m and φ_f have the shape

$$\varphi(\mathbf{u}_s,\alpha_s)=(1-\alpha_s)^2 W(\nabla\mathbf{u}_s)+\frac{\sigma_e^2}{E}\left(\alpha_s+\frac{l^2}{16}(\nabla\alpha_s)^2\right), \qquad (2)$$

where the first term represents the elastic strain energy, with

$$W(\nabla\mathbf{u})=\frac{E}{2(1+\nu)}\left(sym^2\nabla\mathbf{u}+\frac{\nu}{(1-2\nu)}tr\nabla\mathbf{u}^2\right),$$

the elastic energy density of linearly elastic isotropic materials, depending on the Young's modulus E and the Poisson's ratio ν. The second term in (2) is the damage energy as proposed in [21,22]. It is composed of a local term linearly depending on α, and a quadratic non-local function of the damage gradient $\nabla\alpha$. The energy density (2) is proper of brittle materials, which exhibit an initial linearly elastic stage followed by brittle failure. The local stress-strain curve obtained with the energy (2) is drawn in Figure 4a, and the analytical justification of the brittle failure occurring when $\sigma=\sigma_e$ is given in the Appendix, where the equilibrium equations are deduced. The functional (2) depends on the peak stress σ_e, attained at the end of the initial elastic phase, on the Young's modulus E, and on the internal length l, which corresponds to the size of the damage localization zone at fracture. A profile of α in a line x normal to the crack surface is shown in Figure 4b, (see the Appendix for the analytical expression of $\alpha=\alpha(x)$, and [30] for a thorough study).

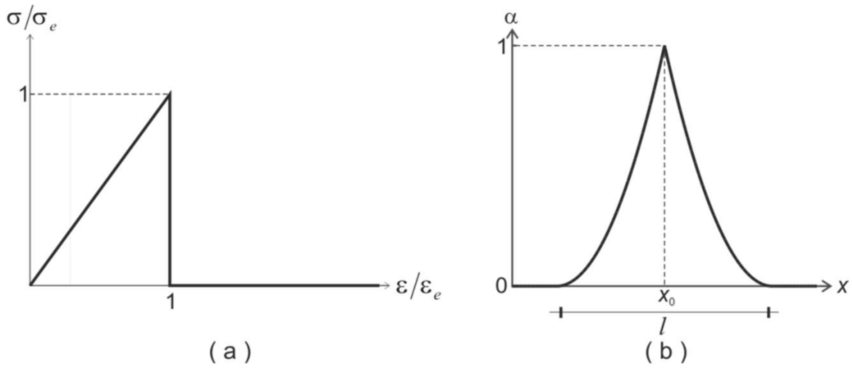

Figure 4 - (a) Stress-strain curve for brittle materials (cementitious matrix and carbon yarn); (b) damage profile on a transversal section of a crack surface.

(ii) Matrix-to-yarn interface energy density

The third term of (1) is the energy of the matrix-to-yarn interface Λ, which has the expression

$$\varphi_\Lambda(\boldsymbol{\delta}_s,\alpha_s)=(1-\alpha_s)^2\frac{1}{2}\mathbf{K}\boldsymbol{\delta}_s\cdot\boldsymbol{\delta}_s+w(\alpha_s)+\tau_0\alpha_s^2\,|\boldsymbol{\delta}_s\cdot\mathbf{t}|\cdot \qquad (3)$$

The first term is the elastic energy density, where the elastic tensor $\mathbf{K}$ is supposed to be diagonal, i.e., $\mathbf{K}=k\mathbf{I}$, with k the elastic coefficient and $\mathbf{I}$ the identity tensor. The degradation function $(1-\alpha_s)^2$ is equal to that assumed in (2).

The second term is the damage energy density, which assumes the following two possible forms

$$w_B(\alpha_s) = \frac{\tau_e^2}{k}\left(\alpha_s - \frac{1}{2}\alpha_s^2\right), \qquad w_D(\alpha_s) = \frac{\tau_e^2}{k}\alpha_s. \tag{4}$$

They are quadratic and linear polynomials of α whose graphs are plotted in Figure 5a, and they depend on the maximum elastic shear stress τ_e, and on the elastic coefficient k. In section 4.2, it is shown that the quadratic expression properly describes brittle debonding, as observed in experiments with dry yarns, while the linear expression is suitable for reproducing ductile debonding, as exhibited by impregnated yarns. Accordingly, indices B and D in (4) stand for brittle and ductile.

Finally, the third term in (3) represents the frictional energy density, whose expression is similar to that proposed in [23,24] to model plastic slip flow. It depends on α and on the absolute value of the tangential slip $\boldsymbol{\delta}_s \cdot \mathbf{t}$, being $\mathbf{t}$ the unit vector tangent to the interface. The constitutive parameter to be assigned in the frictional energy density is the frictional shear stress τ_0.

3.2 Debonding and frictional sliding at the interface

In order to describe the damage evolution associated to the energy density (3), the equilibrium equations in Λ have been determined, when the two faces in contact are subjected to the relative constant load $\mathbf{f}$. In this case, the total energy of Λ is

$$\mathsf{L}(\boldsymbol{\delta},\alpha) = \int_\Lambda \varphi_\Lambda(\boldsymbol{\delta},\alpha)da - \int_\Lambda \mathbf{f}\cdot\boldsymbol{\delta}da, \tag{5}$$

where the second integral is the potential energy of the external load, and index s is omitted. Equilibrium is obtained by requiring the first variation of the total energy (5) to be non-negative for any perturbation, that is,

$$\delta\mathsf{L}(\boldsymbol{\delta},\alpha;\boldsymbol{\mu},\beta) = \int_\Lambda [\frac{\partial\varphi_\Lambda}{\partial\boldsymbol{\delta}}(\boldsymbol{\delta},\alpha)\cdot\boldsymbol{\mu} + \frac{\partial\varphi_\Lambda}{\partial\alpha}(\boldsymbol{\delta},\alpha)\beta]da - \int_\Lambda \mathbf{f}\cdot\boldsymbol{\mu}da \geq 0, \quad \forall\boldsymbol{\mu},\beta, \tag{6}$$

from which the equilibrium relations are

$$\begin{aligned} &\mathbf{f} = (1-\alpha)^2\mathbf{K}\boldsymbol{\delta} + \tau_0\alpha^2\frac{\boldsymbol{\delta}\cdot\mathbf{t}}{|\boldsymbol{\delta}\cdot\mathbf{t}|}\mathbf{t},\\ &\frac{dw(\alpha)}{d\alpha} - (1-\alpha)\mathbf{K}\boldsymbol{\delta}\cdot\boldsymbol{\delta} + 2\tau_0\alpha|\boldsymbol{\delta}\cdot\mathbf{t}| \geq 0. \end{aligned} \tag{7}$$

The first equation is the force-displacement balance equation which is sum of an elastic term and a frictional contribution. When α=0, only the elastic response is active, and $(7)_1$ reduces to $\mathbf{f}=\mathbf{K}\boldsymbol{\delta}$. When α=1, springs are totally broken, and only the frictional force $\mathbf{f} = \tau_0\,\mathrm{sgn}(\boldsymbol{\delta}\cdot\mathbf{t})\mathbf{t}$ survives.

Inequality $(7)_2$ represents the yield condition for damage, according to which damage evolves only when it is satisfied as equality, while elastic evolution is expected when it is satisfied as strict inequality.

If the brittle and ductile damage energy densities (4) are substituted into $(7)_2$, we obtain, respectively,

$$\begin{aligned} &\frac{\tau_e^2}{k}(1-\alpha) - (1-\alpha)\mathbf{K}\boldsymbol{\delta}\cdot\boldsymbol{\delta} + 2\tau_0\alpha|\boldsymbol{\delta}\cdot\mathbf{t}| \geq 0 \text{ (Brittle)},\\ &\frac{\tau_e^2}{k} - (1-\alpha)\mathbf{K}\boldsymbol{\delta}\cdot\boldsymbol{\delta} + 2\tau_0\alpha|\boldsymbol{\delta}\cdot\mathbf{t}| \geq 0 \text{ (Ductile)}. \end{aligned} \tag{8}$$

If a process in which $\mathbf{f}$ monotonically increases is considered, with $\mathbf{f}=\mathbf{0}$ at the initial instant, and the interface is unstressed and undamaged, that is, $\boldsymbol{\delta}=\mathbf{0}$ and $\alpha=0$, then the interface experiences an initial elastic phase whose solution is $\boldsymbol{\delta}=\mathbf{f}/k$ and $\alpha=0$. In this phase, the

inequalities (8) assume the simplified form $\mathbf{f}\cdot\mathbf{f}\le\tau_e^2$, which is strictly satisfied, until the magnitude of $\mathbf{f}$ reaches the value τ_e. Interface debonding initiates when $\mathbf{f}\cdot\mathbf{f}=\tau_e^2$, and it advances in the subsequent instants of the evolution.
Since FRCM systems are usually subjected to shear stresses, we restrict the above problem to pure shear, by assigning the shear stress $\mathbf{f}=\tau\mathbf{t}\ge 0$, and determining the displacement slip $\boldsymbol{\delta}=\delta\mathbf{t}$. Under this assumption, relations (7) simplify as follows

$$\tau=(1-\alpha)^2k\delta+\tau_0\alpha^2,\qquad \frac{dw(\alpha)}{d\alpha}-(1-\alpha)k\delta^2+2\tau_0\alpha\delta\ge 0. \tag{9}$$

By solving equations (9) with respect to δ and τ for varying α in (0,1), it is possible to represent the shear stress versus displacement slip relations. They are plotted in Figure 5b for three different values of τ_0, considering the two energies (4).
After the initial linear elastic phase, the curves exhibit stress-softening, in correspondence of the interface debonding, and damage growth. Then the curves asymptotically tend to the frictional shear stress τ_0. Exception is made by the curve where w_B is implemented and τ_0=0 (red dashed line). In this case, the stress drops down to zero when τ_e is reached. A distinction between brittle and ductile models is that the softening branches (when present) are steeper for w_B than for w_D.
The red curves in Figure 5b describe the local responses assigned to FRCM reinforced with dry (DRY) and pre-impregnated (IMP) yarns. The red curves will be recalled in the next Section 4.4, where the calibration issue is faced.

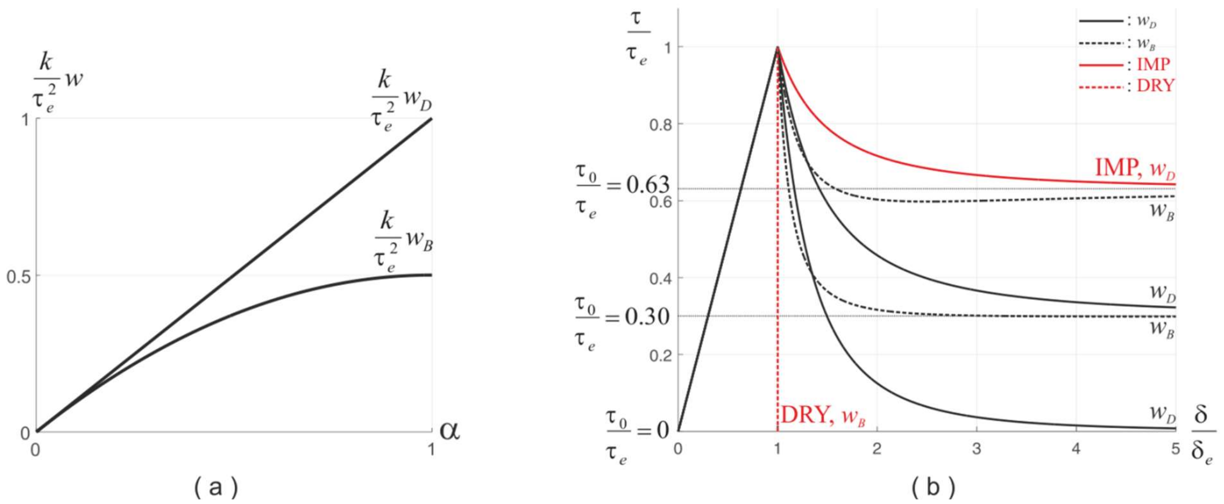

Figure 5 - (a) Graphs of dimensionless damage energy densities w_B and w_D of formula (4). (b) Local shear stress-slip displacement curves in case of energy density w_D (solid line) and w_B (dashed line).

3.3 Evolution problem

In a process where s increases, the evolution of $\mathbf{u}_s$ and α_s is determined by incremental energy minimization [26,27,29]. The loading parameter s is increased through finite steps of size δs, and, within each step, $\mathbf{u}$ and α are supposed to be linear functions of the increment δs

$$\mathbf{u}_{s+\delta s}=\mathbf{u}_s+\frac{d\mathbf{u}_s}{ds}\delta s,\quad \alpha_{s+\delta s}=\alpha_s+\frac{d\alpha_s}{ds}\delta s, \tag{2}$$

and the energy E is developed up to the second order

$$\mathcal{E}(\mathbf{u}_{s+\delta s}, \alpha_{s+\delta s}) = \mathcal{E}(\mathbf{u}_s, \alpha_s) + \frac{d\mathcal{E}(\mathbf{u}_s, \alpha_s)}{ds}\delta s + \frac{1}{2}\frac{d^2\mathcal{E}(\mathbf{u}_s, \alpha_s)}{ds^2}\delta s^2. \quad (3)$$

The rates $(d\mathbf{u}_s/ds, d\alpha_s/ds)$ are determined by minimizing the above functional, under the constrain $d\alpha_s/ds \geq 0$. A finite element code has been developed which implements an alternate iterative minimization procedure, consisting in minimizing the energy functional with respect to the two unknown fields separately.

3.4 Parameters calibration

The constitutive parameters for matrix and yarn are assigned in Table 1. They are the Young's modulus E, the Poisson's ratio ν and the tensile strength σ_e, which are included in the energy density (2).

For the constitutive parameters of the yarn-to-matrix interface, a distinction was made for the dry and pre-impregnated yarn, since the surface treatment strongly influences the bond mechanics. The brittle and ductile energy densities (4) are assigned to DRY and IMP yarns, respectively, and different constitutive parameters are considered, in order to account for the different behaviors observed in pull out tests, as described in Subsection 3.1. The values assigned to τ_e, τ_0, and k are those deduced in Subsection 3.1 from pull out experiments on samples with h=20 mm. To analytically derive them, the hypothesis of homogenous shear stress along the yarn-to-matrix interface is assumed, motivated by the fact that the embedded length is very short. The constitutive parameters assigned to the interface are recall in the following:

- DRY yarn: τ_e=1.40 MPa, τ_0=0 MPa, k=3.10 MPa;
- IMP yarn: τ_e=1.98 MPa, τ_0=1.25 MPa, k=3.95 MPa.

The τ-δ curves obtained by assigning the above parameters are the red curves plotted in Figure 5b. In the case of dry yarn, the behavior is brittle, and a drastic failure is expected when τ_e is reached. In the case of IMP yarn, a pseudo-ductile response is obtained, characterized by a long softening tail asymptotically tending to τ_0.

4. Numerical simulations

In this section, numerical results of pull out and double shear bond tests are presented and compared with experimental evidences. For both pull out and double shear tests, simplified two-dimensional geometries are considered, and the hypothesis of plane strain state is assumed.

The simulations presented below reproduce debonding and slippage at the yarn-to-matrix interface as the unique mechanism leading to failure, which prevails over cracking of the constituents (cementitious matrix and carbon yarn). However, breakage of the constituents has been reproduced in simulations not reported in the paper, by considering different experimental setups (different geometries, loading and boundary conditions).

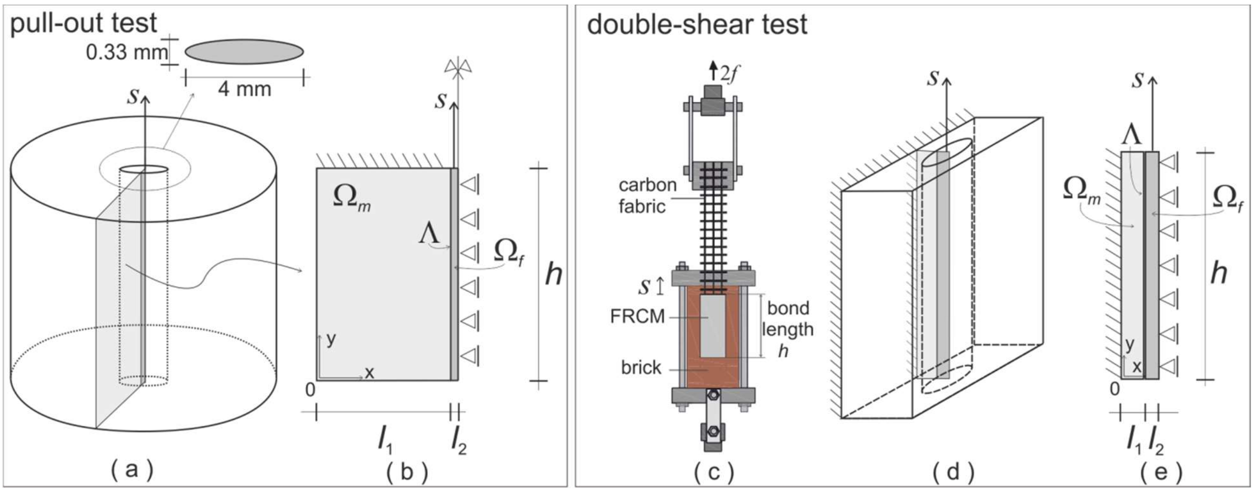

Figure 6 - Sample geometry and two-dimensional scheme of pull out (a,b) and double shear test (c,d,e).

4.1 Pull out tests

The sample geometry of pull out tests is drawn in Figure 6a. One-half sample is considered for symmetry reasons, and the longitudinal section drawn in gray tones is assumed as the two-dimensional domain considered in numerical simulations. Its plane representation is given in Figure 6b. The top side of the matrix domain Ω_m is clamped, and an upward displacement s is applied to the upper side of the yarn Ω_f. The geometrical dimensions are l_1=25 mm, l_2=0.16 mm, and two bond lengths, i.e., h=20, 50 mm, are considered. Simulations are performed for each length, for dry and pre-impregnated carbon yarns.

Force-displacement curves are plotted in Figure 2 (red line). Comparison with experimental results shows excellent agreement between numerical and experimental curves. Simulations accurately capture the peak forces and the different evolution phases observed in experiments.

Evolution of damage and shear stress at the interface of 20 mm thick samples is analyzed in Figure 7, for DRY and IMP yarns, where profiles of α and τ are plotted for different value of s, and different colours are used to distinguish the different phases of the evolution. Dots in the response curves of Figures 7a,d indicate points at which snapshots of α and τ are drawn.

Firstly the brittle failure of the DRY sample is described (Figures 7a,b,c). Looking at the coloured response curve of Figures 7a, three phases can be distinguished: the elastic phase (black), the brittle debonding phase (red) and the final sliding stage (green).

In the initial elastic phase, α=0, and τ grows homogeneously through the interface. When the limit value $\tau=\tau_e$ is reached at the top endpoint of the interface, the debonding process starts, and advances downward. When α=1, any capability of carrying shear stresses is lost. This is due to the fact that the shear stress is null. The debonding front continuously advances up to 1/3 of the interface length, then it dramatically evolves over the entire interface, leading to the complete failure of the sample.

A different evolution process is reproduced in the case of IMP yarn (Figures 7d,e,f). After the initial elastic phase (α=0), which ends when τ has reached the limit value τ_e at the top of the interface, a process of progressive debonding takes place. First, a small amount of damage advances downward. In Figures 7e,f, profiles at s=0.51, 0.52 account for the evolution process of the debonding front. The cusps in the curves of τ, where the shear stress attains the maximum value $\tau=\tau_e$, correspond to the positions assumed by the debonding front. For each profile, points of the interface above the cusp are damaged, while those below are sound. Then α progressively grows homogeneously across the interface. Since shear stress decreases as damage increases, a regime of stress-softening is established. When the asymptotic value τ_0 is approached, the third phase of frictional slippage takes place. In this last stage, damage is practically homogeneous through the interface, assuming the value $\alpha \approx 0.9$. This result is in agreement with the analytical results of Subsect. 3.2, according to which the values $\tau = \tau_0$ and $\alpha = 1$ are asymptotically reached. The transition from debonding to slippage is gradual, with slippage that progressively prevails over debonding.

Finally, brittle (DRY yarn) and ductile (IMP yarn) behaviors can be summarized as follows: a brittle interface experiences only two possible states, sound interface ($\alpha = 0$) and completely debonded interface ($\alpha = 1$); differently, a ductile interface exhibits a cohesive damage evolution where α progressively grows.

Notice that the hypothesis of homogeneous shear stress through the sample, which has been assumed in Section 3.1 to determine τ_e, τ_0 and k (Table 2), is confirmed by simulations, at least in the case of 20 mm in thickness samples. Indeed, as shown by the shear stress profiles of Figure 7, τ is practically constant throughout the interface, with the exception of a very short phase of damage propagation from the top to the bottom of the interface.

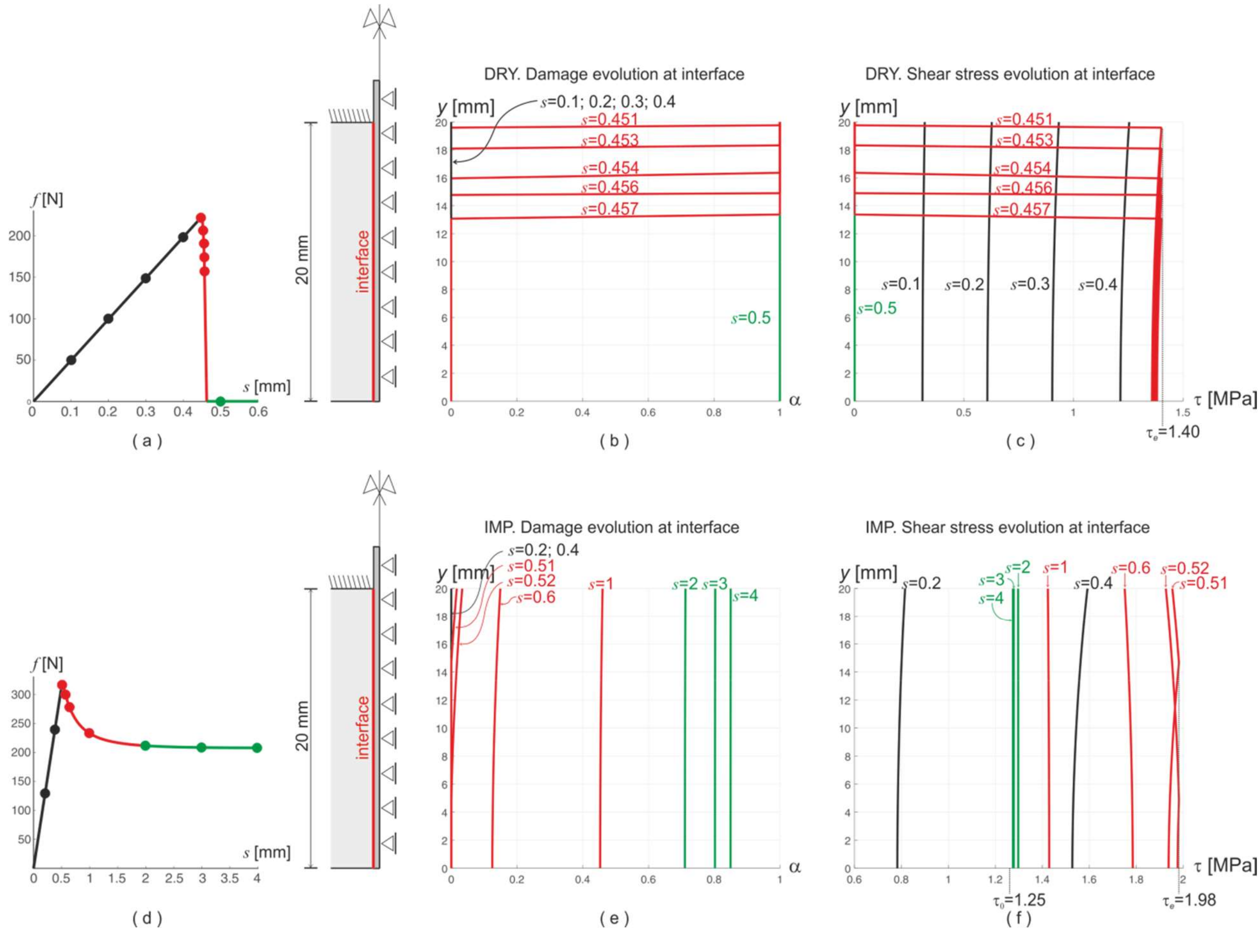

Figure 7 - Pull out tests: profiles of damage α and shear stress τ at the interface for different values of δ (corresponding to the dots in the force-slip curves (a) and (d)). Profiles of α and τ in the case of DRY yarns (b-c); profiles of α and τ in the case of IMP yarns (e-d). [s]=mm.

4.2 Double shear bond tests

The experimental set-up of double shear bond test is shown in Figure 6c, where two FRCM strips are applied on the two sides of a clamped brick. The FRCM system is constituted by the same mortar used in pull out tests, reinforced with dry or pre-impregnated bi-directional carbon fabrics, with 3 longitudinal yarns embedded in the matrix. The carbon fabric is wrapped around a steel cylinder, and it is subjected to a tensile displacement. A sketch of a single yarn surrounded by cementitious mortar is drawn in Figure 6d. The tensile displacement s induces shear stresses at the yarn-to-matrix interface, flowing towards the brick substrate. As discussed in [25], the largest stresses are attained in the sample portion placed between the yarn internal side and the matrix clamped face. For this reason the longitudinal section placed in the middle of this zone is considered. It is highlighted with different gray shades in Figure 6d (light gray for the matrix and dark gray for the yarn), and drawn in Figure 6e. The hypothesis of plane strain state is assumed, justified by symmetry reasons. The lengths l_1=5 mm and l_2=0.22 mm are assigned. Only 2/3 of the total yarn thickness is considered, since it has been assumed that 2/3 of the total tensile force acting on the yarn flows to the matrix through the internal yarn surface, and 1/3 through the external surface. A similar assumption was made in [19].

Simulations are performed by considering DRY and IMP yarns with different bond lengths h. Force-displacement curves are plotted in Figure 8 (red line), where experimental curves for h=50 and 100 mm are added for comparison (black line). Experimental tests with longer bonded lengths will be carried out in future studies.

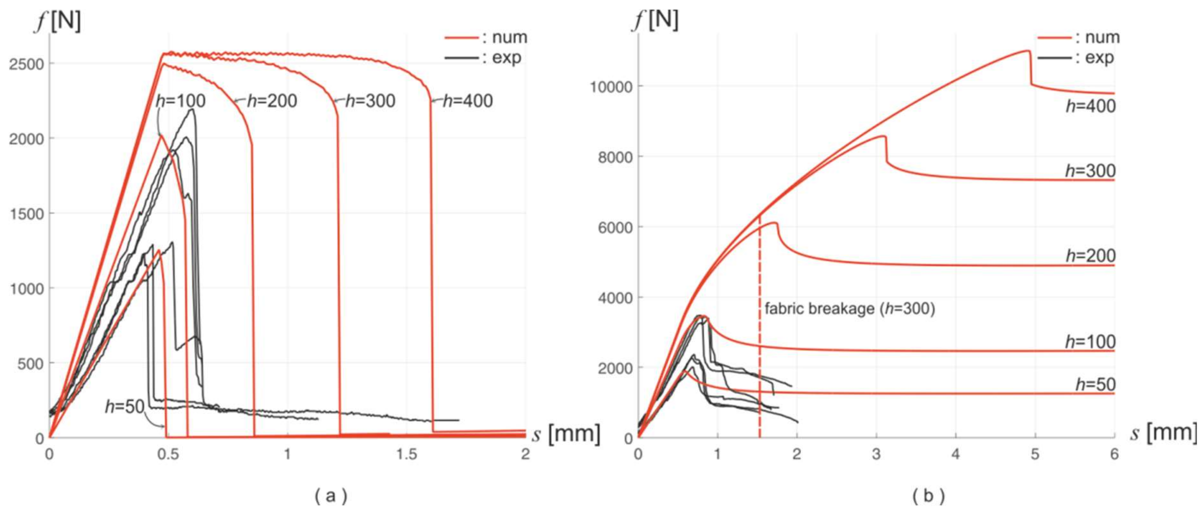

Figure 8 – Double shear bond tests. Experimental and numerical load-displacement curves for different values of the sample bond length. (a) DRY yarns; (b) IMP yarns.

In the case of dry yarn (Figure 8a), curves show an initial linear elastic branch, an intermediate decreasing branch, corresponding to progressive debonding, and a final dropdown branch. Compared with experimental curves where h=50 and 100 mm (three curves for each case), numerical curves provide accurate peak force values, catching the brittle response resulting from experiments. As the sample length increases, the peak force and the slope of the elastic branch increase till the limit value $h \approx 250$ mm. For larger h, neither the maximum force nor the elastic stiffness grow, meaning that 250 mm can be considered the minimum bond length required to properly transfer stresses from the carbon yarn to the substrate.

Curves of Figure 8b are obtained when IMP yarns are considered. In this case, after the initial elastic phase, the debonding stage is described by a stress-hardening curve followed by a shorter stress-softening branch. This latter branch is smooth when low values of h are considered, while it becomes discontinuous for high values of h, exhibiting a dropdown. Curves conclude with frictional plateaus. Comparison with experimental curves (h=50, 100 mm) shows an overestimation of the force in the phase of frictional sliding, especially for h=100 mm. This might be because of transversal yarns that constitute the fabric, which do not contribute to the shear transfer mechanisms at the fabric to mortar interface, remaining attached to the mortar during the slippage of the longitudinal yarns, and thus reducing the effective contact area between longitudinal yarns and matrix. Furthermore, the experimental setup may have induced some instabilities in the post-peak phase, due to the rapid drop of the load carried by the fabric.

Since the peak force increases as h increases, when h>210 mm the tensile stress on a single yarn exceeds the value σ_e=1850 MPa (see Table 1) and the yarn breaks on the top cross-section, where the displacement s is applied. The dashed curve of Figure 8b corresponds to the yarn breakage in a sample of length h=300 mm. Since we are interested in the study of debonding and sliding at the interface, the yarn tensile strength has been increased in order to perform simulations even for longer bond lengths.

Profiles of α and τ at the interface of DRY and IMP samples with bond length h=400 mm are drawn in Figure 9 for different values of s. The evolutions are qualitatively similar to those of pull out tests (Section 5.1). The main difference lies in the fact that τ is no more homogeneous, because of the longer bond length. Looking at the shear stress profiles in the elastic phase, the value of τ decreases going downward through the interface, and the bond length required to transmit the whole tensile force to the matrix is about 250 mm. It is the same bond length deduced from the curves of Figure 8.

In the case of DRY yarn (Figures 9a,b,c), debonding starts at the top endpoint of the interface when the shear stress value τ=τ_e is reached, and then it advances downward. The debonding front proceeds up to 2/3 of the interface length and then it suddenly jumps to the bottom endpoint, leading to the complete separation of the yarn from the matrix.

In the case of IMP yarn (Figures 9d,e,f), the interface is progressively damaged, and the damage front moves down while α grows (see red profiles in Figure 9e). As damage increases, shear stress reduces. In the final phase, damage spreads through the interface, with α=0.80-0.85, and τ tends τ_0.

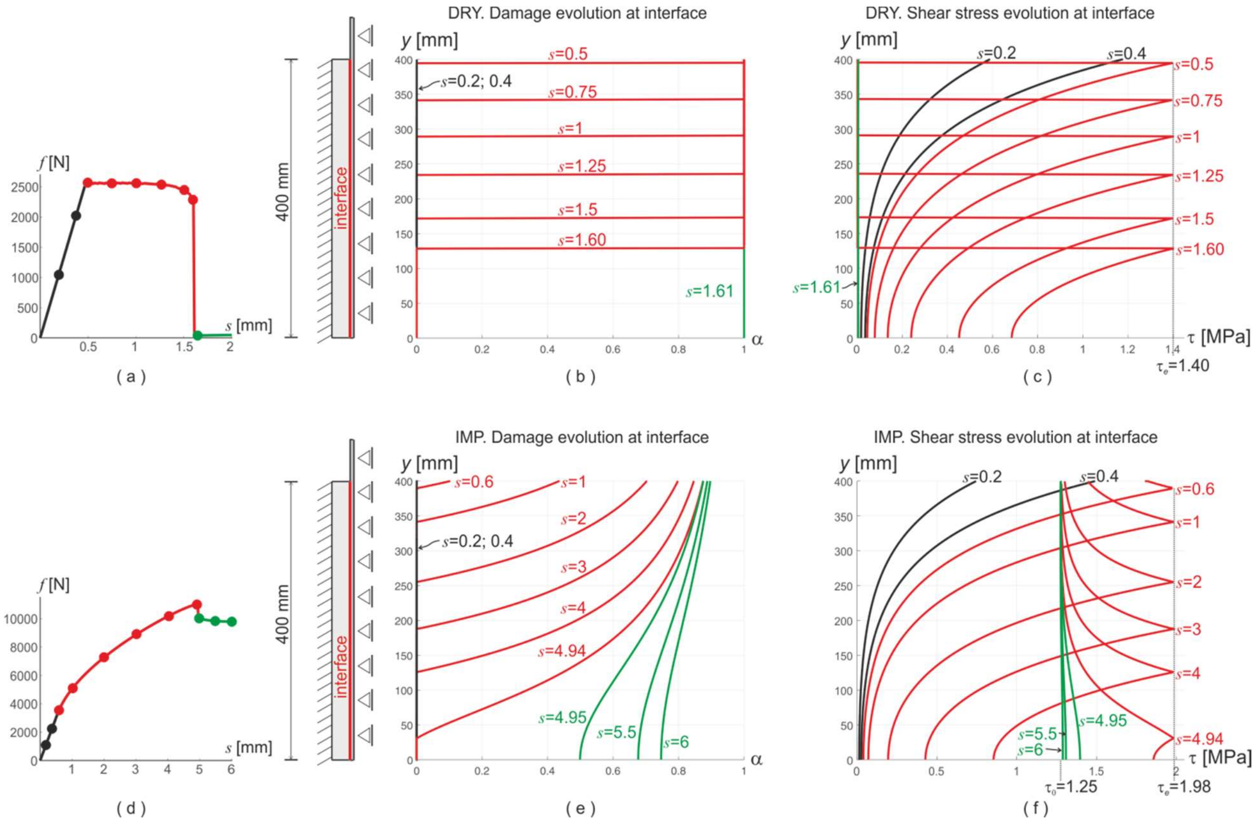

Figure 9 - Double shear bond tests. Profiles of damage α and shear stress τ at the interface for different values of δ (corresponding to the dots in the force-slip curves (a) and (d)). (b-c) profiles of α and τ in the case of DRY yarns; (e-d) profiles of α and τ in the case of IMP yarns. [d]=mm.

5. Conclusions

In this paper, the mechanical behavior and failure modes of multi-filament dry or pre-impregnated carbon yarns embedded in a cementitious matrix are investigated. The bond behavior at the yarn-to-matrix interface is analyzed by means of pull out tests, carried out on single carbon yarns embedded in a cement based mortar for different lengths.
On the basis of the experimental results it was observed a great difference on the mechanical behavior of the samples subjected to pull out tests, depending on the type of carbon yarn used (dry or pre-impregnated with epoxy). The main difference has been observed in the post-elastic phase, when the debonding process starts and evolves. Dry yarns failed in a brittle way once reached the peak load, while pre-impregnated yarns showed a more ductile failure, due to high friction developed at the yarn to matrix interface.
A variational model has been developed in order to provide a thorough understanding of the failure mechanisms for the two different systems. A phase field approach has been followed to formulate the model, where specific internal energies have been assigned to the different components of the system, with the aim of describing the failure modes observed in experiments. Energies accounting for brittle fracture have been assigned to the two FRCM constituents (cementitious matrix and carbon fibers yarn). Special attention was devoted to the definition of the interface energy, in order to reproduce debonding process and slippage at the yarn-to-matrix

interface. Three energetic terms have been assumed, each one contributing to describe a different phase of the evolution; the elastic shear stage, the debonding phase and the final frictional slippage process. Each contribution has a straightforward mechanical meaning, and it has been assigned as simple as possible, with few constitutive parameters, directly related to specific mechanical properties easily measurable from experiments. Thus, the proposed numerical model combined great predictive capability, being able to describe the different stages of the failure processes observed in experiments, and ease of calibration, since the constitutive parameters are related to the experimental data through simple analytical relations.

Numerical simulations have reproduced the FRCM behavior in single or double shear bond tests. In the case of a fabric reinforcement constituted by dry yarns the model allowed to establish an effective bond length of about 200 mm. By further increasing the bond length the maximum load does not increase. FRCM systems reinforced with pre-impregnated carbon fabrics experienced a different behavior. The load increased by increasing the bond length, due to the elevated friction developed in the slippage phase. In this case the failure occurred in the fabric, outside the bonded area.

This study highlighted the potentiality of a variational model to get insight on the mechanical behavior of FRCM systems, in particular at the interface between yarn and matrix, providing a useful numerical tool for the investigation of the effects of geometry and material properties on the mechanical performances of FRCM systems, and on their failure mechanisms.

APPENDIX

Brittle failure of matrix and yarn. In order to better understand the damage evolution associated to the energy density (2) (assigned to matrix and yarn), we consider the simple one-dimensional problem of a bar of length L, subjected to a tensile strain s, and we deduce and discuss the equilibrium equations, referring to [22] for a detailed study including the evolution problem and the stability analysis.

The longitudinal displacement $u=u(x)$ and damage $\alpha=\alpha(x)$, with $x \in (0, L)$, are the problem unknowns. The boundary conditions are $u(0)=0$, $u(L)=sL$, and $\alpha(0) = \alpha(L) = 0$, and the energy density is

$$\varphi(u,\alpha) = (1-\alpha)^2 \frac{1}{2} E u'^2 + \frac{\sigma_e^2}{E}\left(\alpha + \frac{l^2}{16}\alpha'^2\right), \qquad \text{(a)}$$

where $f'(x) = df(x)/dx$. The density (a) is obtained by specializing (2) to the one-dimensional problem of a tensile bar. The tensile stress is $\sigma = (1-\alpha)^2 E u'$, defined as the derivative of the strain energy with respect to the deformation u'. If we impose the first variation of the energy $\int_0^L \varphi(u,\alpha;\delta u,\delta\alpha)dx$ to be non-negative for any admissible perturbation δu and $\delta\alpha \geq 0$, we obtain the equilibrium relations

$$\sigma' = 0, \qquad \sigma \leq \sigma_y = \sigma_e \sqrt{(1-\alpha)^3 \left(1 - l^2 \alpha''\right)}, \qquad \text{(b)}$$

where the first equation is the stress balance equation, which states that σ is constant trough the bar. The second relation is the damage yield condition, and it states that σ can never be larger than the yield stress σ_y. As described in [31], damage evolves when $\sigma = \sigma_y$, while the bar elastically deforms when $\sigma < \sigma_y$.

If the initial configuration of the bar is undamaged and undeformed, and s is monotonically increasing, then the bar experiences an initial elastic stretching, whose solution is $u(x) = sx$, α=0, and $\sigma = Es < \sigma_e$. When the stress attains the value σ_e, inequality (b)$_2$ is satisfied as an equality, and damage can form. As shown in [22], for sufficiently long bars, failure brutally appear in the bar when $\sigma = \sigma_e$, and α jumps from 0 to 1 in a point x_0, decreasing to zero in a neighborhood of x_0 of size l, according to the profile drawn in Figure 1a. The analytical expressions of the profile of α is

$$\alpha = \begin{cases} \left(1 - 2\dfrac{|x - x_0|}{l}\right)^2, & \text{if } |x - x_0| \le l/2, \\ 0, & \text{if } |x - x_0| > l/2, \end{cases}$$

which is determined by integrating (b)$_2$, as described in [30].

REFERENCES

[1] Nanni A. FRCM strengthening e a new tool in the concrete and masonry repair toolbox. *Concrete International*, 2012; 34.

[2] Triantafillou TC, Papanicolaou CG. Shear strengthening of reinforced concrete members with textile reinforced mortar (TRM) jackets. *Materials and Structures*, 2006; 39(1): 93–103.

[3] Corinaldesi V, Donnini J, Mazzoni G. Experimental study of adhesion between FRCM and masonry support. *Key Engineering Materials*, 2015; 624: 189-196.

[4] Raoof SM, Bournas DA. Bond between TRM versus FRP composites and concrete at high temperatures. *Composites Part B: Engineering*, 2017; 127: 150-165.

[5] Minafò G. D'Anna J., Cucchiara C., Monaco A. La Mendola L., Analytical stress-strain law of FRP confined masonry in compression: Literature review and design provisions. *Composites Part B: Engineering*, 2017; 115: 160-169.

[6] Mosallam A.S., Nasr A. Structural performance of RC shear walls with post-construction openings strengthened with FRP composite laminates. *Composites Part B: Engineering*, 2017; 115: 488-504.

[7] Banholzer, B. (2004). "Bond behavior of multi-filament yarn embedded in a cementitious matrix." Ph.D. thesis, Rheinisch-Westfälische Technische Hochschule (RETH) Aachen Univ., Aachen, Germany.

[8] Donnini J, Corinaldesi V, Nanni A. Mechanical properties of FRCM using carbon fabrics with different coating treatments. *Composites Part B: Engineering*, 2016; 88: 220-228.

[9] Donnini J, Corinaldesi V. Mechanical characterization of different FRCM systems for structural reinforcement. *Construction and Building Materials*, 2017; 145(1): 565-575.

[10] Banholzer B, Brameshuber W, Jung W. Analytical simulation of pull-out tests – the direct problem. *Cement and Concrete Composites*, 2005; 27: 93-101.

[11] Banholzer B, Brameshuber W, Jung W. Analytical evaluation of pull-out tests – the inverse problem. *Cement and Concrete Composites*, 2006; 28: 564-571.

[12] Focacci F, D'Antino T, Carloni C, Sneed LH, Pellegrino C. An indirect method to calibrate the interfacial cohesive material law for FRCM-concrete joints. *Materials & Design*, 2017; 128: 206-217.

[13] D'Ambrisi A, Feo L, Focacci F. Experimental analysis on bond between PBO-FRCM strengthening materials and concrete. *Composites Part B: Engineering,* 2012; 44(1): 524–32.

[14] Zhang XB, Aljewifi H, Li J. Failure behavior investigation of continuous yarn reinforced cementitious composites. *Construction and Building Materials*, 2013; 47: 456-464.
[15] Carozzi FG, Colombi P, Fava G, Poggi C. A cohesive interface crack model for the matrix-textile debonding in FRCM composites. *Composite Structures*, 2016; 143: 230-241.
[16] D'Ambrisi A, Feo L, Focacci F. Experimental and analytical investigation on bond between Carbon-FRCM materials and masonry. *Composites Part B: Engineering*, 2013; 46: 15-20.
[17] Ombres L. Analysis of the bond between Fabric Reinforced Cementitious Mortar (FRCM) strengthening systems and concrete. *Composites Part B: Engineering*, 2015; 69: 418-426.
[18] Bencardino F, Condello A, Ashour AF. Single-lap shear bond tests on Steel Reinforced Geopolymeric Matrix-concrete joints. *Composites Part B: Engineering*, 2017; 110: 62-71.
[19] Carloni C, D'Antino T, Sneed LH, Pellegrino C. Role of the Matrix Layers in the Stress-Transfer Mechanism of FRCM Composites Bonded to a Concrete Substrate. *Journal of Engineering Mechanics*, 2015; 141(6).
[20] Marigo JJ, Maurini C, Pham K. An overview of the modelling of fracture by gradient damage models. *Meccanica*, 2016; 51(12): 3107-3128.
[21] Pham K, Amor H, Marigo JJ, Maurini C. Gradient damage models and their use to approximate brittle fracture. *Int. J. Damage Mech*, 2011; 20: 618-652.
[22] Pham K, Marigo JJ, Maurini C. The issues of the uniqueness and the stability of the homogeneous response in uniaxial tests with gradient damage models. *J. Mech. Phys. Solids*, 2011; 59, 1163-1190.
[23] Freddi F, Royer-Carfagni G. Phase-field slip-line theory of plasticity. *Journal of the Mechanics and Physics of Solids*, 2016; 94: 257-272.
[24] Freddi F, Royer-Carfagni G. Plastic flow as an energy minimization problem. Numerical experiments. *J. of Elasticity*, 2014; 116(1): 53-74.
[25] Donnini J, De Caso y Basalo F, Corinaldesi V, Lancioni G, Nanni A. Fabric-reinforced cementitious matrix behavior at high-temperature: Experimental and numerical results. *Composites Part B,* 2017; 108: 108-121.
[26] Del Piero G. A variational approach to fracture and other inelastic phenomena. *J. Elast.,* 2013; 112: 3–73.
[27] Lancioni G. Modeling the Response of Tensile Steel Bars by Means of Incremental Energy Minimization. *J Elast*., 2015; 121: 25-54.
[28] Del Piero G, Lancioni G, March R. A diffuse cohesive energy approach to fracture and plasticity: the one-dimensional case. *J. Mech. Mater. Struct.,* 2013; 8(2-4): 109-151.
[29] Lancioni G, Yalcinkaya T, Cocks A. Energy-based non-local plasticity models for deformation patterning, localization and fracture, Proceedings of the Royal Society A, 2015; 471.
[30] Pham K, Marigo JJ. From the onset of damage to rupture: construction of responses with damage localization for a general class of gradient damage models. *Continuum Mech. Thermodyn*., 2013; 25: 147-171.
[31] Lancioni G, Corinaldesi V. Variational modelling of diffused and localized damage with applications to fiber-reinforced concretes. *Meccanica*, article in press, 2017, DOI: 10.1007/s11012-017-0709-y.